Available online at www.sciencedirect.com

ScienceDirect

Advances in Space Research 61 (2018) 1025–1034

ADVANCES IN SPACE RESEARCH (a COSPAR publication)

www.elsevier.com/locate/asr

Total column water vapor estimation over land using radiometer data from SAC-D/Aquarius ☆

Javier Epeloa *, Amalia Meza

Facultad de Astronomia y Ciencias Geofisicas, Universidad Nacional de La Plata, Argentina

Received 5 March 2017; received in revised form 27 October 2017; accepted 19 November 2017
Available online 26 November 2017

Abstract

The aim of this study is retrieving atmospheric total column water vapor (CWV) over land surfaces using a microwave radiometer (MWR) onboard the Scientific Argentine Satellite (SAC-D/Aquarius). To research this goal, a statistical algorithm is used for the purpose of filtering the study region according to the climate type.

A log-linear relationship between the brightness temperatures of the MWR and CWV obtained from Global Navigation Satellite System (GNSS) measurements was used. In this statistical algorithm, the retrieved CWV is derived from the Argentinian radiometer's brightness temperature which works at 23.8 GHz and 36.5 GHz, and taking into account CWVs observed from GNSS stations belonging to a region sharing the same climate type. We support this idea, having found a systematic effect when applying the algorithm; it was generated for one region using the previously mentioned criteria, however, it should be applied to additional regions, especially those with other climate types.

The region we analyzed is in the Southeastern United States of America, where the climate type is Cfa (Köppen - Geiger classification); this climate type includes moist subtropical mid-latitude climates, with hot, muggy summers and frequent thunderstorms. However, MWR only contains measurements taken from over ocean surfaces; therefore the determination of water vapor over land is an important contribution to extend the use of the SAC-D/Aquarius radiometer measurements beyond the ocean surface. The CWVs computed by our algorithm are compared against radiosonde CWV observations and show a bias of about −0.6 mm, a root mean square (rms) of about 6 mm and a correlation of 0.89.

Keywords: Water vapor; Microwave radiometer; SAC-D/Aquarius; Brightness temperature

1. Introduction

Atmospheric water vapor plays a crucial role in radiative balance and the hydrological cycle (Turco, 1992). Its continuous changes in phase leads to cloud formation and transfer of latent heat from the sea surface (Salby, 2007). Most atmospheric moisture is held within the first 2 km since this is near the source of water from the earth's oceans and land surfaces. Water vapor is the most abundant greenhouse gas (Kiehl and Kevin, 1997), and it is related to climate change and global warming (Hall and Manabe, 2000; Held and Brian, 2006; Trenberth et al., 2006) and has high spatial and temporal variability (Van Baelen et al., 2011). The traditional water vapor measurement techniques are radiosonde and radiometer observations. Radiosonde is a meteorological instrument widely used for routine observations of atmospheric parameters. However, its measurements are not satisfactory regarding space-time resolution since the radiosonde measurements

☆ Fully documented templates are available in the elsarticle package on CTAN.

* Corresponding author at: Paseo del Bosque s/n, Buenos Aires, Argentina.
E-mail addresses: jepeloa@fcaglp.unlp.edu.ar (J. Epeloa), amalia.meza@gmail.com (A. Meza).

https://doi.org/10.1016/j.asr.2017.11.023
0273-1177/

are made once or twice daily at a limited number of stations (Rocken et al., 1995; Wang et al., 2007). Radiosondes provide vertical profiles of temperature, pressure, and relative humidity allowing an estimation of the total column water vapor (CWV) which characterizes the region around a ground station (Rocken et al., 1995; Wang et al., 2007; Pramualsakdikul et al., 2007).

Microwave radiometers observations from earth or satellital missions allow measurement of water vapor directly with a temporal resolution in a range of seconds and better accuracy than radiosondes in the case of surface observations, however, this technique is not effective during raining conditions (Güldner, 1999).

Passive methods for retrieving CWVs exploit the water vapor absorption in three spectral bands, the solar reflectance band between approximately 0.9 μm and 1 μm, the infrared band between approximately 6.5 μm and 8.7 μm and the microwave (MW) band, typically in the absorption lines of 1.35 cm and 1.64 mm (corresponding to frecuencies of 22.2 GHz and 183 GHz). Over land, CWV estimations from MW satellite instruments contain errors of about 6 mm with a linear correlation coefficient of 0.9, and the CWV errors are about 2 mm over the ocean surface (Deeter, 2007).

Analyzing data computed from the Global Navigation Satellite System (GNSS) is another technique used to obtain CWVs based on the GNSS signal's tropospheric path delay. Dense, permanent GNSS ground tracking networks were established around the world during the past thirty years and the use of them to estimate CWVs has been widely extended to various weather regimes and diverse climate regions; thus constituting the basis of GNSS Meteorology (Bevis et al., 1992; Duan et al., 1996).

In this manuscript we will focus on radiometer measurements from space. A satellite-borne radiometer observing the Earth is sensitive to radiance emanating from land surfaces and the atmosphere.

CWVs can be retrieved by applying three types of algorithms: statistical, physical, and semi-statistical (Wang et al., 2009; Sohn and Smith, 2002). A statistical algorithm similar to Wang et al.'s (2009) was employed in this study with one modification: CWVs from GNSS observations over land are used, hereafter CWV_{GNSS}, instead of microwave radiative transfer simulations for CWVs over the sea surface. Then, our results are compared with CWVs obtained from radiosonde observations (hereafter CWV_{RAOB}).

This paper has been divided into five parts. The data section presents the datasets employed in our work and the retrieval algorithm section develops the algorithm used. The results are presented in section four, and finally, the conclusions and discussions are presented in section five.

2. Data

The Scientific Argentine Satellite (SAC-D/Aquarius) mission is a cooperative international scientific mission developed between the USA's National Aeronautics and Space Administration (NASA) and the National Commission of spacial activities (CONAE) of Argentina, with participation from the Italian Space Agency (Agenzias paziale Italiana, ASI), the French Space Agency (Centre National d'Etudes Spatiales, CNES), and the Canadian Space Agency (CSA).

Fig. 1 displays the microwave radiometer (MWR) instrument located inside the SAC-D/Aquarius satellite; it consists of two radiometers operating at K and Ka bands. Each radiometer is connected to a set of eight feed-horns arranged in two rows of four feeds illuminating a parabolic torus reflector. The ground footprints for two rows lie on two different conical arcs with incidence angles of 52 and 58 degrees.

The reflectors are scaled to match the secondary antenna pattern's 3 dB beam width at both frequencies. The most common 3 dB beam-width is 1.64°, resulting in Instantaneous Field of View (IFOV) with a resolution of 50 km on the ground. Each row of feed-horn produces IFOVs lying in a conical arc on the ground.

The MWR's datasets contain (in version 4 of CONAE or version 6 from CFRSL) L1.B information, which provides the radiometer's brightness temperature readings. These datasets have corrected smear effect and non-linearity gain.

The algorithm employed in this work focuses on CWV retrieval under non-precipitating conditions; therefore, the precipitation detection are made using cloud coverage information from weather database provided by the University of Wyoming (http://weather.uwyo.edu/surface/meteorogram). Cloud coverage information requires clear sky conditions when the satellites pass over the GNSS station are used.

CWV_{GNSS} data are stored in the SuomiNet database (http://www.suominet.ucar.edu/) which is one of the most important GNSS tracking networks in the World (Ware et al., 2000).

CWV_{GNSS} data and the corresponding MWR brightness temperature readings, are used to perform a log-linear regression to obtain the adjustment coefficients, as explained in the next section.

CWV_{GNSS} data and the MWR measurements collected between January and September 2014 over a region of the USA are matched with a spatial difference less than 50 km from the ground GNSS station. To avoid coastal contamination of the MWR measurements, only CWV_{GNSS} within the continent's boundaries are used

CWV_{RAOB} data derived from the Wyoming international database are compared with the retrieved CWV, hereafter CWV_{Cal}. The CWV_{RAOB} data are matched with the brightness temperature measurements of MWR at 12 h universal time (UTC).

Fig. 2 shows the 37 GNSS stations' locations (Table 1) used to perform the algorithm and Fig. 3 shows the 10 radiosonde launch sites (Table 2) selected to compare with our results.

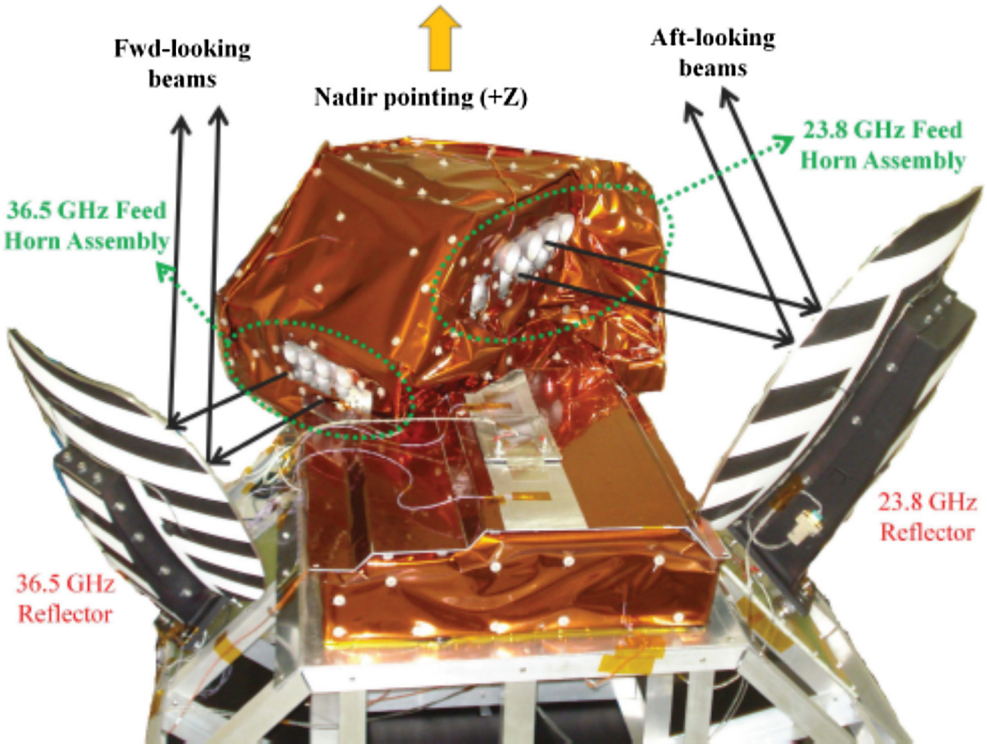

Fig. 1. MWR radiometer Sayak Krishna Biswas (2009).

Fig. 2. Selected GNSS stations.

The region where we perform the algorithm was selected while taking into account the Köppen - Geiger (hereafter K-G) climate classification (Peel et al., 2007) in this case, it is a warm temperate climate (type Cfa) and is located between 30°N and 40°N latitude, and −100°E to −85°E longitude in North America. This region was also chosen because GNSS, radiosonde data, and the footprint of MWRs have enough temporal and spatial coincidences,

Table 1
Selected GNSS stations.

Station name	Latitude [°]	Longitude [°]	Mean PWV value [mm]	Available Points
AL20	34.71032	−87.6627	16.28	14
AL30	33.532351	−86.8534	18.02	15
AL50	33.167974	−87.5015	20.05	15
AL60	32.411374	−86.2705	18.28	17
AL70	31.782747	−85.9652	19.97	18
ARBT	35.709875	−91.6285	15.91	16
ARHP	33.696055	−93.6006	15.05	6
ARPG	36.059114	−90.5188	15.46	18
HGIS	34.728111	−86.5867	16.94	15
MCN5	32.695324	−83.5606	21	18
MLF5	32.090261	−87.3918	19.06	15
MSB5	34.11452	−90.6903	16.39	19
MSME	32.367512	−88.7324	19.21	14
P777	35.70266	−92.5455	14.61	18
P778	35.240351	−85.8149	10.17	7
P779	35.201941	−82.8725	9.51	14
SG01	36.604141	−97.4848	16.3	19
SG04	37.131915	−97.2661	16.03	20
SG08	36.841334	−96.428	7.51	10
SG09	36.430752	−98.2844	14.94	19
SG10	36.881427	−98.2864	17.58	15
SIHS	31.843383	−91.6554	19.49	18
TXAB	32.503258	−99.7568	13.42	20
TXDC	33.236223	−97.6087	19.61	18
TXHM	31.699489	−98.1067	16.72	20
TXLF	31.356351	−94.7183	24.5	16
TXMA	32.535318	−94.2886	22.86	16
TXPA	33.674236	−95.557	22.28	15
GACC	33.545758	−82.1338	18.48	13
KYTK	37.151455	−83.7596	15.23	15
MOKE	36.221425	−90.0735	17	17
P805	32.963237	−84.2258	19.5	18
SAL5	35.367078	−94.8166	22.96	11
TXBU	30.750461	−98.1844	18.32	18
TXTY	32.249616	−95.3936	23.04	15

especially for the last two cases, allowing us find a solution as will be explained later.

3. Methodology

3.1. Retrieval algorithm

All retrieval algorithms have advantages and disadvantages; the statistical algorithm is computationally simple, however, no representative selection of a reference CWV dataset could introduce retrieval differences for each statistical algorithm, and the lack of physical constraints makes this kind of model reliable only in regions where environmental conditions are similar to those used to train the algorithm. However, the physical algorithms strongly depend on the radiative transfer equation to determine the relationship between the brightness temperature (here after T_b) and CWV. The advantage of this algorithm is the capability of identifying very small changes in atmospheric moisture, but this ability is limited by the empirical and illusive simplified assumptions employed. Finally, semi-statistical algorithms are a mix of statistical and physical algorithms because they use regression formulas to relate the T_b and CWV, but employ the radiative transfer equation.

In our research, we use the statistical algorithm account for the type of climate based on its K-G classification; more specifically, the algorithm is computed for a region with homogeneous climatic conditions. K-G (Peel et al., 2007) proposes a climate classification which takes into account variations in temperature and humidity as the averages of the warmer or colder months and emphasizes the bioclimatic consequences. Therefore, this system is based on the concept that native vegetation is the best expression of climate. The selection of a restricted area is also supported by the results of Deeter, who in 2007 Deeter (2007) concluded that over land, vegetation distribution is an important factor affecting the retrieved CWVs' dispersion.

The algorithm proposed in this work is formulated as a two-chanel log-transform (T_s bias), multiple-linear regression (Wang et al., 2009). Wang et al. explained the principle for the CWV retrieval algorithm, assuming the atmosphere is isothermic (Deeter and Vivekanandan, 2006) and no rain conditions exist, then the CWV can be determined by log-linear regression regarding brightness temperatures:

Fig. 3. Selected RAOB stations.

Table 2
Selected radiosonde launch sites.

Station name	Latitude [°]	Longitude [°]	Mean PWV value [mm]	Available Points
72,215	33.36	−84.57	19.75	18
72,235	32.32	−90.08	7.51	4
72,248	32.46	−93.78	22.15	17
72,249	32.83	−97.3	17.62	20
72,327	36.25	−86.57	15.33	17
72,451	37.76	−99.97	9.26	16
72,440	37.23	−86.57	17.24	17
72,340	34.84	−92.26	14.68	20
72,318	37.2	−80.41	14.79	13
72,317	36.08	−79.95	16.15	14

$$CWV = A_0 + \sum_{i=1}^{n} A_i \mathrm{Ln}\left(\frac{T_s - T_{b_i}}{T_s}\right) \quad (1)$$

where T_{b_i} is the brightness temperature at the ith channel of the radiometer and A_0, A_i $(i = 1, .., n)$ and T_s are adjustment coefficients.

To account for the horns' incidence angle, we estimate the algorithm's coefficients of Eq. (1) for the even and odd beams (which correspond to 58°and 52°respectively). The adjustment produces two sets of coefficients of Eq. (1) for the MWR's two angles of incidence.

The MWR has two bands at 23.8 GHz (horizontal polarization) and 36.5 GHz (vertical and horizontal polarization). Among all the possible combinations of frequencies and polarizations in Eq. (1), we found the best-fit is obtained using the 23.8 GHz and 36.5 GHz vertical polarizations in this case, the upper bound of yhe summation in Eq. (1) is two. Replacing the Observed MWR and GNSS water vapor data in Eq. (1) can be written as:

$$CWV = A_0 j + A_1 j \mathrm{Ln}\left(\frac{T_s j - T_{b_{23.8}}}{T_s j}\right) + A_2 j \mathrm{Ln}\left(\frac{T_s j - T_{b_{36.5}}}{T_s j}\right) \quad (2)$$

In Eq. (2), the unknown coefficients $A_i j$ (i = 0,1,2, j = even, odd) and $T_s j$ (j = even, odd) can be solved by using a non-linear least square method. The CWV from GNSS and the respective values of each brightness temperature ($T_{b_{23.8}}$ and $T_{b_{36.5}}$) are obtained by taking the averaged values of these measurements in a circular region with radius equal to 50 km from the GNSS ground station.

Using external brightness temperatures sources during the pre-launch calibration test, it was found the SACD/Aquarius MWR receivers have a compressive non-linearity

for brightness temperatures over 300 K. The receiver is compressing high input power signals from landmasses causing systematic low deflection counts for these scenarios (Sayak Krishna Biswas, 2009). Therefore, to avoid the possibility of non-linearities, measurements of brightness temperatures larger than 300 K are eliminated.

The estimation model was performed over a region of the USA, with the same climate type. At this point, we emphasize the selected analysis region is characterized by the presence of many GNSS stations belonging to the same climate type, has many radiosondes launching points close to the GNSS stations, and finally,there are enough footprints of the MWR onboard the SACD that are simultaneous with both kinds of observations.

3.2. Köppen - Geiger climate division

To estimate the amount of total column water vapor over land we used the Köppen - Geiger climate division (Kottek et al., 2006; Rubel et al., 2017) to obtain the coefficients of the Eq. (2) this paper's main contribution. The Köppen - Geiger (K-G) climate classification scheme divides climates into five main groups (A, B, C, D, E), each having several types and subtypes; the second letter indicates the seasonal precipitation type, while the third letter indicates the level of heat. Each particular climate type is represented by a two- to four-letter symbol.

This climate division account for the amount of vegetation covering the land which is considered one of the more important source of systematic bias in the regression coefficients (Eq. (2)), owing to a deviation in the background brightness temperature is produced, which is translated to the adjustment. K-G climate division allow us considering the background's effect when estimating the coefficients and fit the algorithm so it is associated with a particular region.

The estimation model was performed in a region of USA with a climate type designation of Cfa, which belongs to the humid subtropical climate. The world maps of K-G climate classification is located at the web address: http://koeppen-geiger.vu-wien.ac.at/. At this point, we emphasize the selected analysis region has the characteristic Of containing many GNSS stations belonging to the same climate type, has many radiosondes launching points close to the GNSS stations and finally,there are enough footprints of the MWR onboard SACD that are simultaneous with both kinds of observations.

To analyze the algorithm's performance, we proposed applying it to different regions and different time periods; therefore, five GNSS stations over South-America were analyzed in a period between January to September of the year 2013, Table 3.These regions belong to different K-G climate types. The BRAZ station has an Aw climate type or tropical with dry winter, and the POVE station has an Am climate or tropical monsoon and the PARC has a Cfc climate, or subpolar oceanic climate. The CWV measurements were obtained by Bianchi et al. (2016), whose data files can be found at the website address: https://doi.pangaea.de/10.1594/PANGAEA.858234. The authors compared the quality of these results with radiosonde measurements and found it to be similar to those obtained by other authors (Wang et al., 2007). The mean values of the difference, between CWV from radiosonde and GNSS are within/+1 mm and their standard deviations are below 3 mm. These CWV_{GNSS} measurements were compared with our results, CWV_{Cal}, obtained using the adjusted coefficients and the corresponding brightness temperatures from MWR data onboard the SAC-D. This analysis shows the influence of the climate classification as criteria needed to obtain a regional algorithm using Eq. (1).

Table 3
Selected Stations in South-America region.

Latitude [°]	*Longitude* [°]	*Climate Type*	*Station Name*
−27.36	−55.89	**Cfa**	EBYP
−22.12	−51.41	**Cfa**	PPTE
−15.94	−47.87	AW	BRAZ
−53.13	−70.88	BSk	PARC
−8.71	−63.90	AM	POVE

4. Results

4.1. Estimation of algorithm coefficients

The CWV_{GNSS} values from 37 GNSS stations belonging to the SuomiNet Network, and their respective brightness temperatures are used in Eq. (2) to obtain the unknown coefficients and T_s; Table 4 presents their values:

Figs. 4 and 5 show a scatter plot of the brightness temperatures and the CWV_{GNSS} for even and odd beams used to derive the regression coefficients.

Therefore, the CWV_{Cal} can be obtained using the coefficients (Table 4) and the brightness temperatures in both bands from Eq. (2).

Fig. 6 shows the scatterplot for CWV_{Cal} and CWV_{GNSS} values, using the data obtained during an eight months period (from 1 Jan 2014 to 31 August of 2014). The standard deviation and the correlation coefficient are 6.47 mm and 0.87, respectively.

The value of STD is mainly affected by the variability of land emissivity; this emissivity is strongly related to the surface characteristics (for instance, the vegetation), in this manuscript, the region of analysis is selected taking in account the climate region criteria to minimize this effect. We observed in the Fig. 6 that for CWV values smaller than 20 mm the algorithm slightly overestimate, and for

Table 4
Unknowns of the retrieval algorithm coefficients.

Beams	A_0	A_1	A_2	T_s
Even	−51.48 [mm]	−29.03 [mm]	−2.66 [mm]	300 [°K]
Odd	−49.74 [mm]	−24.71 [mm]	−4.99 [mm]	297 [°K]

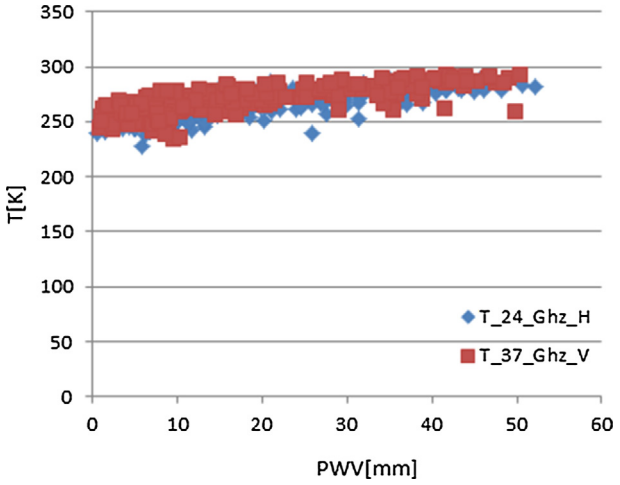

Fig. 4. Scatterplot with T_b and CWV_{GNSS} for odd beams.

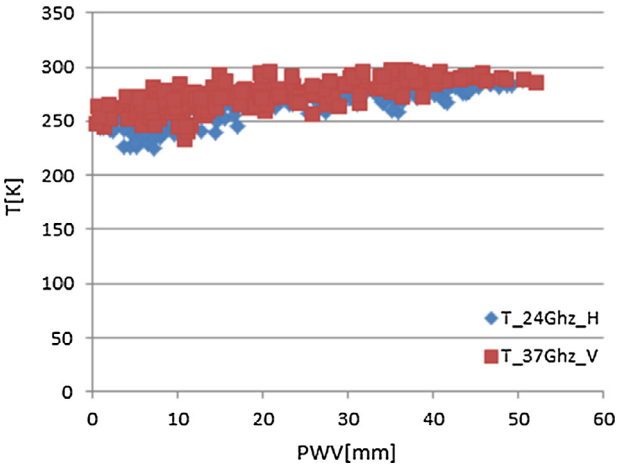

Fig. 5. Scatterplot with T_b and CWV_{GNSS} for even beams.

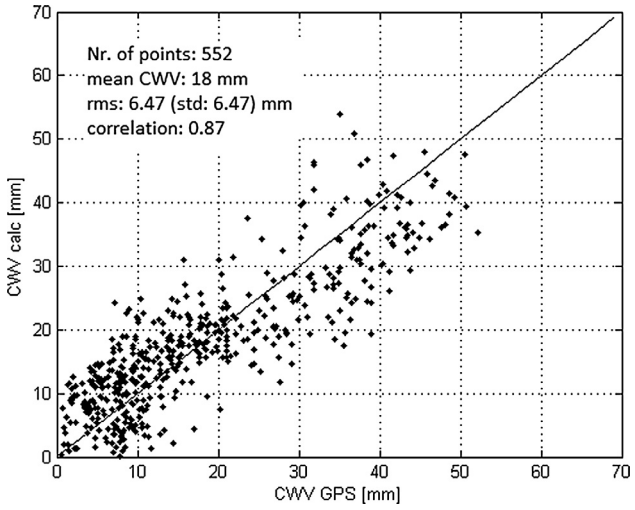

Fig. 6. Result of estimation model.

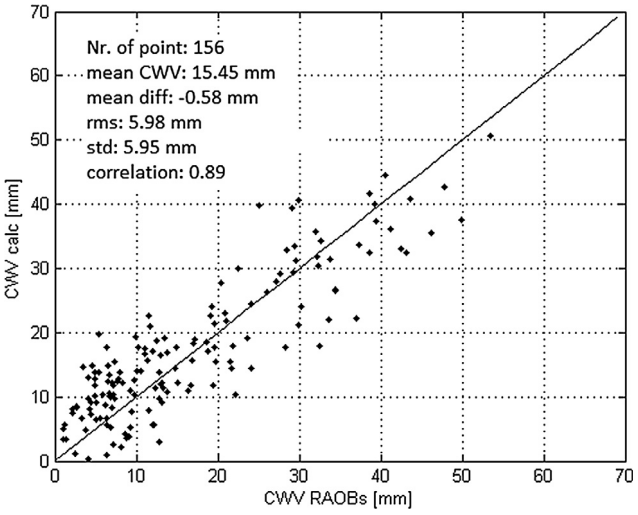

Fig. 7. Comparison between CWV_{Cal} and CWV_{RAOB}.

values of CWV larger than 20 mm, the algorithm slightly underestimated the CWV.

4.2. Comparison with CWV obtained by radiosonde

The CWV_{Cal} values obtained with the retrieval algorithm described in the previous subsection, are compared to the values obtained from radiosonde readings in the same region. The radiosonde launch places are not collocated with GNSS stations (Tables 1 and 2); only three of them are close to GNSS stations.

The MWR's brightness temperatures, $T_{b_{23.8}}$ and $T_{b_{36.5}}$ that match with the CWV_{RAOB} observation in a circle less than 50 km from radiosonde launch sites,are replaced in Eq. (2), and using the coefficient of Table 4, the CWV are computed, named CWV_{Cal}.

Therefore, the mean value of the difference (mean diff.) between CWV_{RAOB} and CWV_{Cal}, its standard deviation (STD), and its root mean square (rms) are calculated.

Fig. 7 shows the result of the comparison. It can be observed that the mean diff. is −0.59 mm; this difference could be explained by, among other factors, the systematic difference between CWV_{GNSS} (taking into account that the coefficients were computed with CWV_{GNSS} observations) and CWV_{RAOB} (from VAISALA radiosonde) found by other authors such as Wang and Zhang (2008).

The standard deviations (STD) are smaller than 6 mm and this not surprising due to the uncertainties in CWV radiosonde determination and the brightness temperature measurement errors although the more important effect could be attributed to the variability of land emissivity, even taking into account this effect was minimized using the same climate type for the analyzed region.

4.3. Comparison with CWV obtained by GNSS station located in different regions

Figs. 8–12 show the agreement between the CWV values from different stations in the GNSS, and the CWV_{Cal}

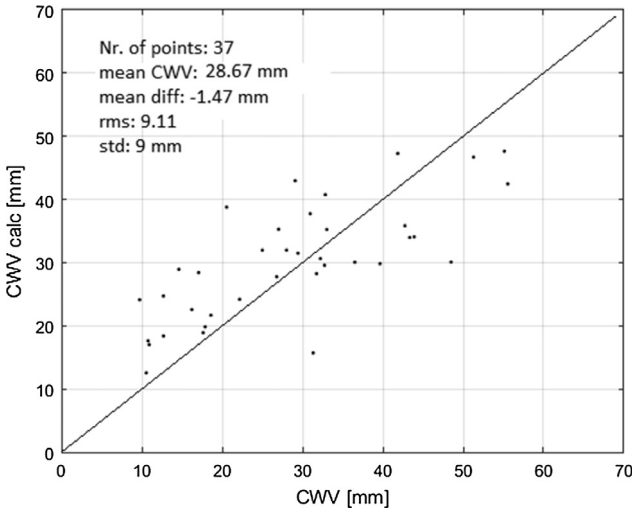

Fig. 8. Validation over EBYP GNSS Station.

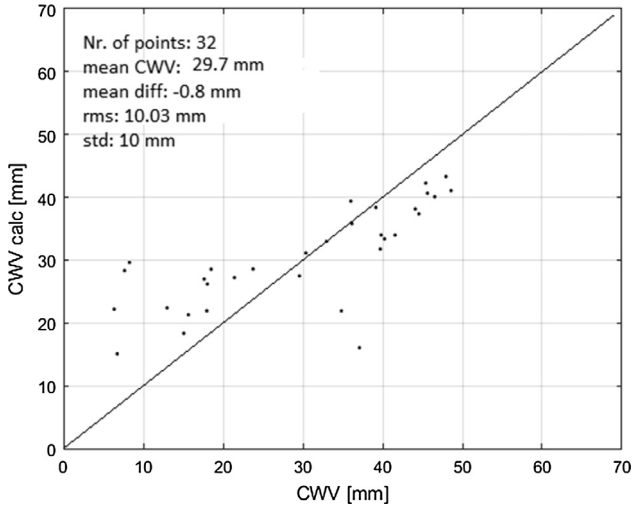

Fig. 9. Validation over PPTE GNSS Station.

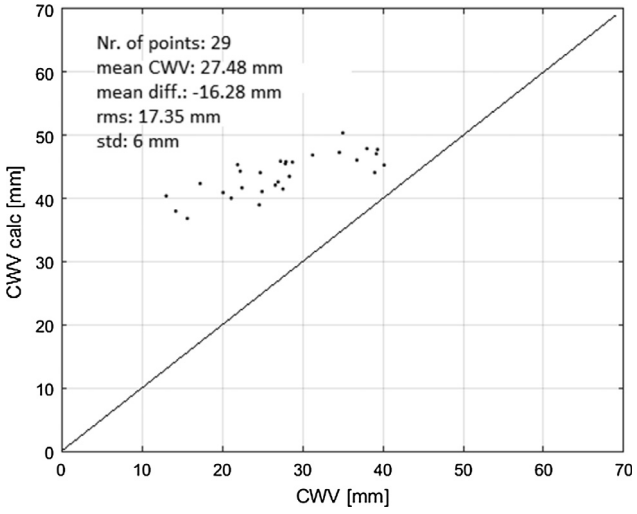

Fig. 10. Validation over BRAZ GNSS Station.

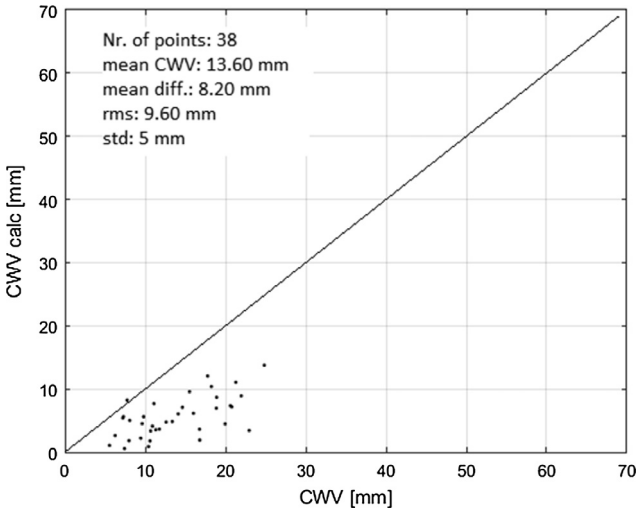

Fig. 11. Validation over PARC GNSS Station.

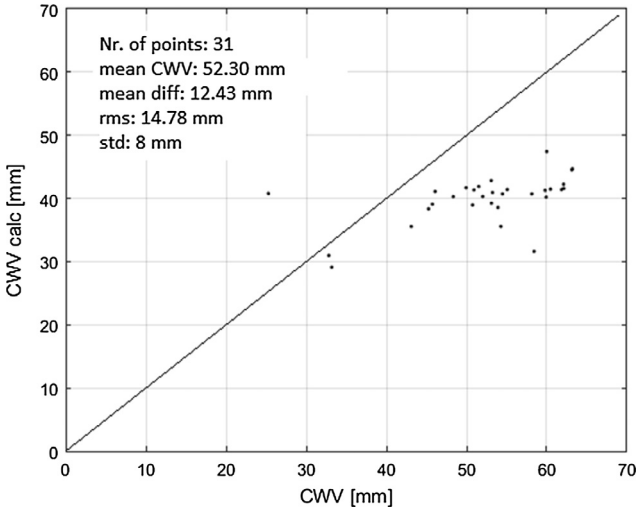

Fig. 12. Validation over POVE GNSS Station.

obtained using the statistical algorithm proposed in this work, with the coefficients obtained previously (Table 4). These figures present the scatter plot (CWV_{GNSS} and CWV_{Cal}) for GNSS stations with different climate types. For those with climate classification similar to the analyzed region, the mean difference is smaller than those obtained for stations with different climate types.

Fig. 13 shows an example of a CWV map generated from Eq. (2) and coefficients of Table 4. This map is created using the data from week 16 of the year 2014.

The results obtained in the Figs. 8–12 support the idea that it is very important to consider the climate type when the algorithm Eq. (2) is implemented; if it not, systematic differences could be commented on. The absolute value of the mean of differences between calculated CWVs and CWVs from GNSS. The GNSS station within the climate region Cfa, shows strong agreement, lower than 1.5 mm,

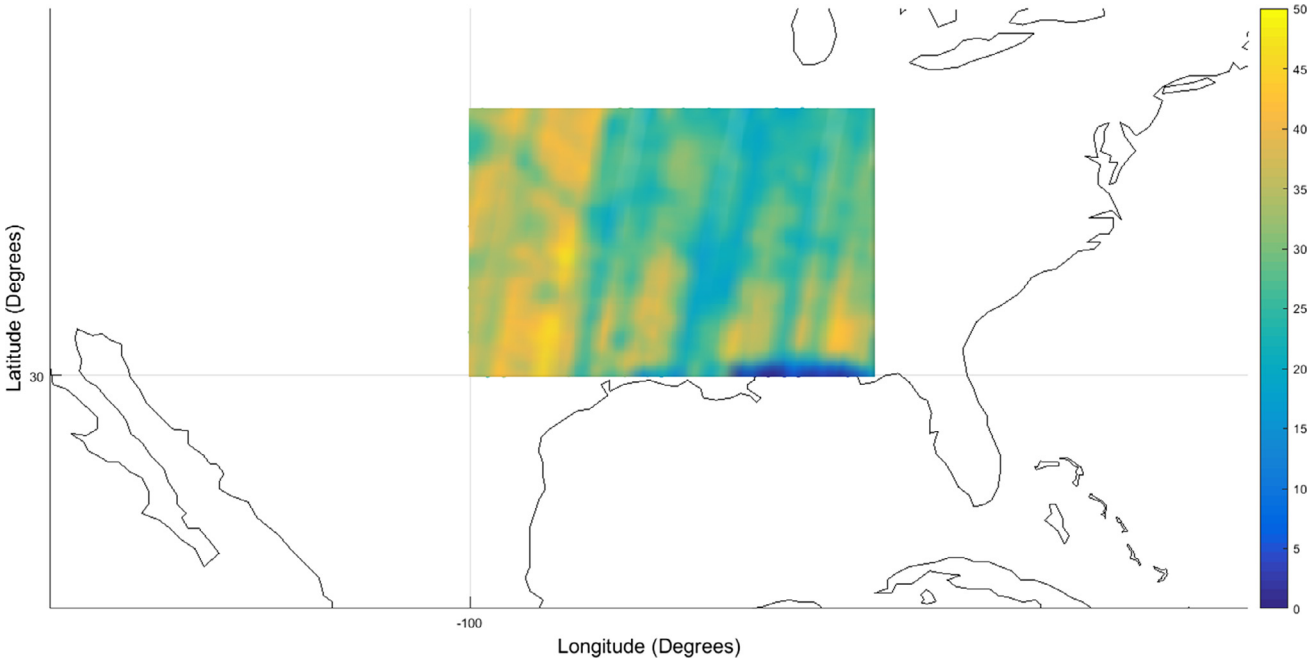

Fig. 13. Regional map of CWV using the calibrated proposed model.

but for the station with different climate types, the values are larger than 8 mm.

5. Conclusion

In this paper, we present an algorithm to retrieve CWV over land using the brightness temperature of the radiometer MWR onboard the SAC-D/Aquarius mission and the CWV_{GNSS} observations. The criteria employed to select the region to implement the algorithm is the Köppen - Geiger climate classification. In our manuscript, the chosen area is the Central- Southeastern region of the USA with the clime type Cfa (warm temperature climates) where there is wide coverage of GNSS and radiosonde observations, and there are enough footprints of the MWR onboard the SACD Coinciding with these observations.

We propose a log-linear algorithm in terms of brightness temperatures at 23.8 GHz and at 36.5 GHz to obtain CWVs in this region. The unknown of the algorithm are fitted by the non-linear least square method. Finally, the standard deviation (STD) between CWV_{GNSS} and CWV_{Cal} is 6.47 mm and the correlation is 0.87.

The CWV_{Cal} is compared with CWV_{RAOB}; the mean difference between both CWV values is −0.59.mm, and its rms is about 6 mm. Our algorithm slightly under- and over- estimate the CWV values when it is lower and higher than about 20 mm, respectively. Similar results were observed by other authors who work in centimeter and micrometric wave longitudes (Sohn and Smith, 2002; Fernandez et al., 2010). Only the CWV values over ocean surfaces is provided by the SAC-D/Aquarius mission. Therefore our results, based on the determination of the CWVs over land, are an important contribution to extend the use of the SACD-D/Aquarius measurements beyond the ocean surface.

This work proposes a statistical algorithm whose set of coefficients are calculated in a region taking into account the climate classification of the stations that provide CWV observations. The observable's used for the adjustment, is obtained from the GNSS, but radiosonde or other equipment capable of providing CWV observations could also be used, always taking into account the MWR onboard of the satellite SAC-D/Aquarius footprint intersects the location of the observable in order to measure the respective brightness temperature.

Acknowledgements

This research is supported by an ANPCyT grants PICT 2012-1484 and PIP2012 00292. The authors thank the Argentine Comision Nacional de Actividades Espaciales (CONAE) for providing the radiometer data.

References

Bevis, M., Businger, S., Herring, T.A., Rocken, C., Anthes, R.A., Ware, R.H., 1992. GPS meteorology: remote sensing of atmospheric water vapor using the global positioning system. J. Geophys. Res.-Atmos. 97, 15787–15801. https://doi.org/10.1029/92JD01517.

Bianchi, C.E., Mendoza, L.P.O., Fern/andez, L.I., Natali, M.P., Meza, A. M., Moirano, J.F., 2016. Multi-year GNSS monitoring of atmospheric IWV over central and South America for climate studies. Ann. Geophys. 34, 623–639. https://doi.org/10.5194/angeo-34-623-2016.

Deeter, M.N., 2007. New satellite method for retrieving precipitable water vapor over land and ocean. Geophys. Res. Lett. 34, L02815. https://doi.org/10.1029/2006GL028019.

Deeter, M.N., Vivekanandan, J., 2006. New dual-frequency micro- wave technique for retrieving liquid water path over land. J. Geophys. Res. 111, D15209. https://doi.org/10.1029/2005JD006784.

Duan, J., Bevis, M., Fang, P., Bock, Y., Chiswell, S., Businger, S., Rocken, C., Solheim, F., van Hove, T., Ware, R., McClusky, S., Herring, T.A., King, R.W., 1996. GPS meteorology: direct estimation of the absolute value of precipitable water. J. Appl. Meteorol. 35, 830–838. https://doi.org/10.1175/1520- 0450(1996)035<0830: GMDEOT>2.0.CO;2.

Fernandez, L.I., Salio, P., Natali, M.P., Meza, A.M., 2010. Estimation of precipitable water vapor from GPS measurements in Argentina: validation and qualitative analysis. Advances in Space Research. 46, 879–894.

Güldner, Spänkuch, 1999. Result of year round remotely sensed integrated water vapor by ground based microwave radiometry. J. Appl. Meteorol. 38, 981–988.

Hall, A., Manabe, S., 2000. The effect of water vapor feedback on internal and anthropogenic variations of the global hydrologic cycle. J. Geophys. Res. 105 (D5), 6935–6944.

Held, I.M., Soden, Brian J., 2006. Robust responses of the hydrological cycle to global warming. J. Climate 19, 5686–5699. https://doi.org/10.1175/JCLI3990.1.

Kiehl, J.T., Kevin, E., 1997. Trenberth; Earth's annual global mean energy budget. Bull. Am. Meteorol. Soc. 78, 197–208. https://doi.org/10.1175/1520-0477(1997)078<0197:EAGMEB>2.0.CO.

Kottek, M., Grieser, J., Beck, C., Rudolf, B., Rubel, F., 2006. World map of the Kppen-Geiger climate classification updated. Meteorol. Z. 15, 259–263. https://doi.org/10.1127/0941-2948/2006/0130.

Peel, M.C., Finlayson, B.L., McMahon, T.A., 2007. Updated world map of the Kppen-Geiger climate classification. Hydro. Earth Syst. Sci. 11, 1633–1644.

Pramualsakdikul, S., Haas, R., Elgered, G., Scherneck, H.G., 2007. Sensing of diurnal and semi-diurnal variability in the water vapor content in the tropics using GPS measurements. Met. Appl. 14, 403–412. https://doi.org/10.1002/met.39.

Rocken, C., Van Hove, T., Johnson, J., Solheim, F., Ware, R., Bevis, M., Chiswell, S., Businger, S., 1995. GPS/STORM – GPS sensing of atmospheric water vapor for meteorology. J. Atmos. Oceanic Tech. 12, 468–478.

Rubel, F., Brugger, K., Haslinger, K., Auer, I., 2017. The climate of the European Alps: shift of very high resolution Kppen-Geiger climate zones 1800–2100. Meteorol. Z. 26, 115–125.

Salby, M.L., 2007. The influence of planetary-wave transience on horizontal air motions in the stratosphere. J. Atmos. Sci. 49, 405–421.

Sayak Krishna Biswas. 2009. Brigthness Temperature Calibration of SAC-D/AQUARIUS Microwave Radiometer (MWR) (Ph.D. thesis). University of Central Florida.

Sohn, B.J., Smith, E.A., 2002. Explaining sources of discrepancy in SSM/I water vapor algorithms. J. Climate 16, Nro 20.

Trenberth, K.E., Hurrell, J.W., Stepaniak, D.P., 2006. The Asian monsoon: Global perspective. In: The Asian Monsoon. Springer, New York, pp. 67–87.

Turco, R.P., 1992. Upper atmosphere aerosols: properties and natural cycles. The Atmospheric Effects of Stratospheric Aircraft: A first program Report, Nasa Ref. Pub. 1272, 63–82.

Van Baelen, J., Reverdy, M., Tridon, F., Labbouz, L., Dick, G., Bender, M., Hagen, M., 2011. On the relationship between water vapour field evolution and the life cycle of precipitation systems. Quart. J. Roy. Meteorol. Soc. 137 (S1), 204–223, Online publication date: 1-Jan.

Wang, Junhong, Zhang, Liangying, 2008. Systematic errors in global radiosonde precipitable water data from comparisons with ground-based GPS measurements. J. Climate 21, 2218–2238. https://doi.org/10.1175/2007JCLI1944.1.

Wang, J., Zhang, L., Dai, A., Van Hove, T., Van Baelen, J., 2007. A near-global, 2-hourly data set of atmospheric precipitable water from ground-based GPS measurements, J. Geophys. Res.- Atmos. 112, D11107. https://doi.org/10.1029/2006JD007529.

Wang, X., Auler, A.S., Edwards, R.L., Cheng, H., Ito, E., Wang, Y., Kong, X., Solheid, M., 2007. Millennial-scale precipitation changes in southern Brazil over the past 90,000 years. Geophys. Res. Lett. 34, L23701. https://doi.org/10.1029/2007GL031149.

Wang, Y., Fu, Y., Liu, G., Liu, Q., Sun, L., 2009. A new water vapor algorithm for TRMM Microwave Imager (TMI) measurements based on a log linear relationship, J. Geophys. Res. 114, D21304. https://doi.org/10.1029/2008JD011057.

Ware, R.H., Fulker, D.W., Stein, S.A., Anderson, D.N., Avery, S.K., Clark, R.D., Droegenmeier, K.K., Kuettner, J.P., Minster, J.B., Sorooshian, S., 2000. SuomiNet: a real-time national GPS network for atmospheric research and education. Bull. Am. Meteorol. Soc. 81, 677–694. https://doi.org/10.1175/1520- 0477(2000)081<0677: SARNGN>2.3.CO;2.